Characterisation of hydrous ferric oxides derived from iron-rich groundwaters and their contribution to the suspended sediment of streams

Stijn Baken[a], Carin Sjöstedt[b], Jon Petter Gustafsson[bc], Piet Seuntjens[def], Nele Desmet[d], Jan De Schutter[g], and Erik Smolders[a]*

[a] KU Leuven, Department of Earth and Environmental Sciences, Kasteelpark Arenberg 20 bus 2459, 3001 Heverlee, Belgium, [b] KTH Royal Institute of Technology, Department of Land and Water Resources Engineering, Teknikringen 76, SE-100 44 Stockholm, Sweden, [c] SLU Swedish University of Agricultural Sciences, Department of Soil and Environment, Box 7014, SE-750 07 Uppsala, Sweden, [d] VITO, Boeretang 200, 2400 Mol, Belgium, [e] University of Antwerp, Department of Bioscience Engineering, Groenenborgerlaan 171, 2020 Antwerp, [f] Ghent University, Department of Soil Management, Coupure Links 653, 9000 Ghent, Belgium, [g] Flanders Hydraulics Research, Berchemlei 115, 2140 Antwerpen, Belgium

* Corresponding author, tel. +3216321761, e-mail: stijn.baken@ees.kuleuven.be

NOTICE: this is the postprint version (after peer review) of a work that was accepted for publication in Applied Geochemistry. Changes resulting from the publishing process, such as editing, corrections, and structural formatting may not be reflected in this document. Changes may have been made to this work since it was submitted for publication. A definitive version was subsequently published in Applied Geochemistry 39 59-68 (2013), DOI 10.1016/j.apgeochem.2013.09.013

Abstract

When Fe(II) bearing groundwaters surface in streams, particulate authigenic Fe-rich material is produced by oxidation. Such freshly precipitated Fe minerals may be transported as suspended sediment and have a profound impact on the fate of trace metals and nutrients in rivers. The objective of this study was to monitor changes in mineralogy and composition of authigenic material from its source to streams of increasing order. Groundwaters, surface waters, and suspended sediment in streams of different order were sampled in the Kleine Nete catchment (Belgium), a lowland with Fe-rich groundwaters (3.5—53.8 mg Fe/L; pH 6.3—6.9). Fresh authigenic material (> 0.45 µm) was produced by oxidising filtered (< 0.45 µm) groundwater and surface water. This material contained, on average, 44 % Fe, and smaller concentrations of C, P, and Ca. Iron EXAFS (Extended X-ray Absorption Fine Structure) spectroscopy showed that the Fe was present as poorly crystalline hydrous ferric oxides with a structure similar to that of ferrihydrite. The Fe concentration in the suspended sediment samples decreased to 36—40 % (stream order 2), and further to 18—26 % (stream order 4 and 5). Conversely, the concentrations of organic C, Ca, Si, and trace metals increased with increasing stream order, suggesting mixing of authigenic material with suspended sediment from a different source. The Fe speciation in the suspended sediment was similar to that in fresh authigenic material, but more Fe-Fe interactions were observed, *i.e.* it was increasingly hydrolysed, suggesting ageing reactions. The suspended sediment in the streams of order 4 and 5 is estimated to contain between 31 % and 59 % of authigenic material, but more data are needed to refine this estimate. The authigenic material is an important sink for P in these streams which may alleviate the eutrophication risk in this catchment.

1. Introduction

Iron (Fe) strongly affects the geochemistry of many rivers worldwide. In anoxic environments, the highly soluble Fe(II) is generally the most stable redox form. The rate of the oxidation reaction to Fe(III), which dominates in oxic environments, strongly depends on pH. The turnover time is typically a few hours in oxic waters at circumneutral pH, and slower under more acidic conditions (Davison and Seed, 1983). The solubility of Fe(III) is low since it hydrolyses (e.g. $Fe(III) + 3H_2O \rightarrow Fe(OH)_3 + 3OH^-$) and forms poorly crystalline hydrous ferric oxide (HFO). Dissolved organic matter (DOM) can mobilise Fe(III) and Fe(II) through complexation or through stabilisation of colloidal HFO (Karlsson and Persson, 2012; Lofts et al., 2008; Sjöstedt et al., 2013). However, at elevated total Fe concentrations, HFO particles become larger in size and precipitate. As a result, dissolved (< 0.45 µm) Fe concentrations exceeding 2 mg/L are exceptional in oxic European surface waters (Salminen, 2005).

Where Fe(II)-rich groundwaters surface and become oxic, they may locally cause extensive production of HFOs in the aquatic environment. The presence of such material is often witnessed by reddish brown sediment at the bottom of e.g. drainage ditches or small brooks (see Supplementary Material, Fig. S5). This Fe-rich material is termed authigenic, because it is generated in the river, as opposed to allochthonous material (e.g. eroded riverbank particles) which has a different origin. The structure, size, and morphology of aquatic Fe minerals depend on the pH, the DOM concentration and properties, the presence of micro-organisms, and the concentration of inorganic ligands (Châtellier et al., 2004; Perret et al., 2000). Iron-rich authigenic material has been identified as ferrihydrite or lepidocrocite (Rhoton et al., 2002) and may contain quantitatively important concentrations (above 1 wt %) of other elements such as organic C, Ca, and P (Gunnars et al., 2002; Lienemann et al., 1999). These elements are either incorporated or adsorbed. The authigenic Fe-rich material may strongly influence the fate and availability of elements that have a high affinity for HFOs and

that typically occur at low dissolved concentrations, such as P, As, Ni, Pb, V (e.g. Dzombak and Morel, 1990; Huser et al., 2011; Wällstedt et al., 2010). Especially the effect of Fe-rich authigenic material on P, which may be incorporated at molar ratios down to Fe:P = 2 or even lower (Gunnars et al., 2002; Hyacinthe and Van Cappellen, 2004), is expected to have large implications for many freshwater systems: reducing dissolved P concentrations has often been shown successful in counteracting eutrophication (Schindler, 2012).

As Fe-rich authigenic material is generated in the aquatic environment, it becomes part of the sediment. It is mixed with allochthonous material, i.e. particles that have a different origin. The sediment material is then subjected to processes of aggregation, settling, and resuspension. It may be transported downstream as suspended sediment, especially at high discharge after storm events (Vanlierde et al., 2007). It may settle again in rivers further downstream or ultimately in estuaries, where most of the suspended Fe-rich material is expected to aggregate and settle due to the increased salinity (Boyle et al., 1977). In some cases, authigenic material may represent a significant fraction of the total suspended sediment load, and increase the need for dredging in navigable waterways. Knowledge on the fate of authigenic material is, therefore, of interest to waterway managers and contributes to a better understanding of sediment transport in rivers.

Vanlierde et al. (2007) studied the transport of authigenic material in the Kleine Nete catchment, a catchment with a flat topography, acid sandy soils, and Fe-rich groundwaters. They estimated its annual export at between 58 and 96 % of the total suspended sediment export. This estimation was based on a sediment transport model calibrated to total suspended solids, including effects of settling, burial, consolidation, and resuspension of the sediment. However, they only briefly discussed the formation and geochemistry of Fe-rich authigenic material, and the study lacked samples of authigenic material.

The goal of the present study was, therefore, to explore the geochemistry of authigenic Fe-rich material at catchment scale. In particular, this study was set up to identify changes in mineralogy and elemental composition of suspended authigenic material on its way from groundwaters to small brooks and, ultimately, to the major rivers. We used EXAFS (Extended X-ray Absorption Fine Structure) spectroscopy to characterize the coordination environment of Fe. The formation of authigenic Fe-rich material was simulated by allowing Fe(II)-bearing groundwaters to oxidise. The produced authigenic material was compared with samples of suspended sediment from streams of increasing order. The working hypothesis is that the Fe(II) in streams is oxidised to Fe(III), and that the resulting authigenic material is increasingly diluted by mixing with allochthonous material and by adsorption reactions.

2. Materials and methods

2.1 The study site

The Kleine Nete catchment (Belgium) upstream of Grobbendonk was selected as the study area. The geology, geography and hydrology of this catchment cause elevated and highly variable Fe concentrations in groundwaters, and the subsequent formation and transport of important amounts of authigenic Fe-rich material in the aquatic environment (Vanlierde et al., 2007). The geological setting of the Kleine Nete catchment consists of thick tertiary deposits which are overlain by a thin layer of Quaternary material. Some Tertiary layers, most notably the Diestiaan formation, combine high concentrations of glauconite, a Fe-K phyllosilicate mineral, with a high permeability. Upon weathering of glauconite, Fe is released to the anoxic groundwaters (Courbe et al., 1981) which is present as reduced Fe(II). In a previous study, the dissolved Fe concentration averaged 14.6 mg/L (median: 4.5 mg/L; P_{10}—P_{90}: 0.6—38.8 mg/L) across 313 samples from shallow (< 1 m) groundwaters at four locations in the Kleine Nete catchment (Van Laer and Smolders, 2013). The soils receive organic matter, N, and P which originate from agricultural inputs and which may leach to the groundwater. The phreatic groundwater tables are generally shallow and fluctuate seasonally.

The contribution of groundwater to the total discharge of the Kleine Nete is estimated between 62 and 87 %. The high groundwater contribution is a result of the flat topography, which limits overland runoff and erosion, and the presence of drainage ditches adjacent to agricultural fields, which readily allow surfacing and export of shallow groundwaters. As Fe-rich groundwaters surface and are oxidised, large amounts of authigenic Fe-rich material are produced in the aquatic environment. This material may then be transported downstream as suspended sediment. The water column and the top 1—3 cm of the sediment of rivers in the Kleine Nete catchment generally are oxic (Vlaamse Milieumaatschappij VMM, 2013), which

limits the importance of reductive dissolution of authigenic material. The Fe-rich material may also accumulate in topsoils: bog iron ore occurs in the Kleine Nete catchment and has been mined for its iron (De Geyter et al., 1985). In summary, the conditions in the Kleine Nete catchment promote the formation and transport of large amounts of authigenic Fe-rich material.

2.2 Sampling

Three sampling locations in the Kleine Nete catchment were selected. These were located in the Slootbeek (stream order 2, a small brook with deep-red bottom sediment), in the Aa (stream order 4, a major tributary to the Kleine Nete), and in the Kleine Nete (stream order 5). Samples were collected at four occasions (sampling events S1—S4) between October 2011 and June 2012. Detailed maps of the sampling sites, pictures, meteorological conditions, and discharge data recorded at the time of the sampling events are available in section 1 of the Supplementary Material.

Samples of groundwater, surface water, and suspended sediment were collected. Between 25 and 50 L of groundwater was sampled at approximately 5 m from the watercourse using a peristaltic pump and a fully screened temporary well installed with Geoprobe®. The direct-push approach of the Geoprobe® ensures minimal disturbance, and groundwater could be sampled shortly after the installation of the well. The sampling depth was between 2.8 and 3.8 m below the ground level and depended on the local hydrogeology, *i.e.*, the feasibility to pump at an appreciable rate without entry of air bubbles. The groundwater was discarded during the first 5 minutes and was then collected in plastic vessels that were continuously flushed with N_2 in order to minimise oxygen entry. The collection of groundwater generally took between 1 and 3 hours. Approximately 50 L of surface water was sampled with a bucket and was stored in plastic vessels. Subsamples of groundwater and surface water were filtered

in the field (nitrocellulose membrane filters, 0.45 µm pore size, 25 mm diameter, Whatman) and immediately acidified to pH 2 with HCl in order to stabilise the Fe redox speciation. The suspended sediment of the Kleine Nete and Aa was isolated with a field centrifuge (Emmie, Alfa Laval). This device allows the collection of sufficient suspended material from rivers even if suspended sediment concentrations are low. Surface water is continuously pumped by an immersion pump into the rotating centrifuge where most of the particulate material is collected at the walls and the clear water exits through the centre. The pump inlet was positioned at about 0.7 m above the bed and 0.5 m below the water surface. As the inlet area of the pump is relatively large, it is assumed that little or no particle segregation occurred near the inlet. Collection of sufficient suspended sediment typically took between 1 and 3 hours. The use of the field centrifuge was not necessary in the Slootbeek due to the high suspended sediment concentration. The suspended material was collected by sampling the water with a bucket and by centrifugation upon return to the lab. Upon return to the lab, all samples were stored at 4 °C prior to further processing. The suspended sediment samples were freeze-dried and also stored at 4 °C. The composition of water samples was measured by the ferrozine method (Fe(II); Viollier et al. (2000)), ICP-OES (Fe and other elements), catalytic combustion (DOC), and anion chromatography as described in section 2 of the Supplementary Material. The composition of suspended sediment samples was determined by oxidative digestion (C and N), by ICP-OES after digestion in boiling *aqua regia*, and by Energy Dispersive X-ray Fluorescence (ED-XRF). Details about these procedures are presented in section 2 of the Supplementary Material.

2.3 Oxidation experiments

The oxidation of Fe(II) and the production of authigenic material in natural water samples were simulated in order to identify the production of authigenic material. There were seven different treatments (Table 1). The prefiltered treatments with groundwater (A), surface water

(B), mixed groundwater and surface water (C), and surface water with added Fe(II) (D) simulated the production of authigenic material. The treatments with unfiltered water samples (E—G) tested the effect of the presence of particles and micro-organisms on the oxidation rate of Fe(II). Treatment G contained formalin, a biological poison previously used in a similar context (Tipping et al., 1989), and was included to test the contribution of biotic oxidation reactions which may be important even at circumneutral pH (de Vet et al., 2011).

The oxidation experiments were set up within 20 hours after sampling. During this storage period, some oxidative losses of Fe occurred (see section 3 of the Supplementary Material). Immediately before the start of the experiment, subsamples of groundwater and surface water (between 10 and 30 L) were prefiltered using two successive filters: a 5 µm polypropylene filter (Macrowind, Van Borselen filters, Zoetermeer, the Netherlands) and a 0.45 µm polypropylene-borosilicate filter (AC BX, Atlas Filtri, Limena, Italy). The prefiltration allowed oxygen entry into the groundwater samples which explains why, at the start of the experiment, even the treatments with only groundwater (A) contained dissolved oxygen concentrations above 6 mg/L in all but one instances. Shortly after the prefiltration, oxidation experiments were set up in transparent plastic pots, each containing a total volume of 800 mL. At least two replicates were prepared for each treatment. The treatments spiked with Fe(II) were prepared by adding an aliquot of a freshly prepared 10 g Fe(II)/L solution ($FeSO_4 \cdot 7H_2O$ dissolved in 10^{-5} M HCl) which yielded final Fe(II) concentrations between 5 and 50 mg/L. This increased the ionic strength of such treatments by between 0.36 and 3.6 mM. The formalin treatments were prepared by adding an aliquot of formalin stock (37 % formaldehyde in water and 10 % methanol) to yield a final formalin concentration of 2.5 g/L. All treatments were homogenised and incubated at 15 °C in darkness. They were neither stirred nor aerated during the course of the experiment.

The pH, the dissolved oxygen (DO) concentration, the composition of the dissolved phase, and the concentration and composition of authigenic material were monitored until the oxidation of Fe(II) was nearly complete, which lasted between 8 hours and 3 days after the start of the experiment. During the course of the experiment, the DO concentration did not vary more than 0.8 mg/L in individual treatments, and the pH did not vary more than 0.1 units, except for some treatments with only surface water (treatment B). The dissolved phase was sampled in duplicate (nitrocellulose membrane filters, 0.45 µm pore size, 25 mm diameter, Whatman), and the dissolved concentrations of Fe(II) (ferrozine method), Fe and other elements (ICP-OES), and DOC (catalytic combustion) were measured as described in section 2 of the Supplementary Material. After homogenisation of the experimental solutions, the authigenic material was isolated in duplicate by passing between 100 and 400 mL over pre-weighed filters (nitrocellulose membrane filters, 0.45 µm pore size, 47 mm diameter, Whatman) under vacuum. The filter with the isolated authigenic material was dried (105 °C), weighed, and the composition of the authigenic material was determined by ICP-OES after digestion in *aqua regia* as described in section 2 of the Supplementary Material.

2.4 EXAFS spectroscopy

The iron speciation in two authigenic samples and in three suspended sediment samples (Table 3) was determined by EXAFS spectroscopy. The three suspended sediment samples were collected during S1 in the Kleine Nete, Aa, and Slootbeek; their isolation was described in section 2.2. The two samples of authigenic material were produced in the oxidation experiments (section 2.3) with water samples collected at the Aa river during S2. These samples were isolated (nitrocellulose membrane filters, 0.45 µm pore size, 47 mm diameter, Whatman) from treatment A (prefiltered groundwater) and treatment C (mixture of prefiltered groundwater and surface water) after 48 hours of oxidation. The filters were freeze dried and the samples were removed from the filters with a spatula. The samples were stored at 4 °C.

Iron K-edge (7112 eV) EXAFS spectra were recorded at the wiggler beamline I811 at MAX-lab, Lund, Sweden. All EXAFS samples were mounted in aluminium holders and fixed with Kapton tape. The spectrum of a metallic iron foil was used for energy calibration. Because of a defective I_2 detector, the foil was run after every other sample. The storage ring was operated at 1.5 GeV (maximum ring current 230 mA). Beamline I811 was equipped with a Si[111] double crystal monochromator. Higher-order harmonics were reduced by detuning the second monochromator crystal to reflect approximately 40 % of the maximum intensity at the end of the scans. The I_0 and I_1 detectors were 300 mm-long ion chambers (FMB-Oxford). The fluorescence detector was a passivated implanted planar silicon (PIPS) detector. More details on beamline I811 are provided by Carlson et al. (2006). The scans were recorded at ambient temperature in fluorescence mode with a Mn filter between the sample and the detector. For each sample, between 10 and 15 scans were recorded. No gradual changes were observed in subsequent scans, indicating that the sample was well preserved throughout the measurement.

Data processing and modelling was performed using the Athena and Artemis programs, respectively, which are both included in the IFEFFIT program suite (Ravel and Newville, 2005). In Athena, all scans of a sample were aligned which caused an energy shift of at most 0.05 eV. The scans were averaged and deglitched. The energy of the resulting spectrum was calibrated using the spectra of metallic Fe foil which were recorded after every other sample. A value of 7112 eV was assigned to the first inflection point of the Fe foil spectrum. The pre-edge region was fitted with a linear function which was subtracted from the data. The background was removed with the Autobk algorithm which is included in Athena using a *k*-weight of 2 and a rbkg parameter of 1. In order to optimise the background removal, a first-shell fit of the EXAFS spectrum was set as standard for background subtraction. The resulting spectrum was exported to Artemis for modelling. It was Fourier-transformed using a Hanning window between 2 and 12.5 $Å^{-1}$. The EXAFS model (described in the next paragraph) was

fitted to the real part of the Fourier transform between 1 and 4 Å, and fits were optimised across *k*-weights of 1, 2, and 3. According to the Nyquist theorem ($N_{max} = 2\ \Delta k\ \Delta R\ \pi^{-1}$, with Δk the *k*-range of the EXAFS spectrum and ΔR the R-range considered), the amount of independent points in each spectrum was 20.

Because all EXAFS spectra resembled that of ferrihydrite, an atomic structure was assumed with Fe in a octahedral configuration to six O atoms at distances close to 2.00 Å, and with two Fe—Fe distances in the second and third coordination shells at approximately 3.03 and 3.43 Å. The former Fe—Fe distance refers to edge-sharing Fe octahedra, whereas the latter is attributed to double corner-sharing Fe octahedra (Toner et al., 2009). Based on this atomic structure, a model for the EXAFS signal was deduced which included single scattering Fe—O and triangular Fe—O—O multiple scattering paths in the first coordination shell, a Fe—Fe2 single scattering path (for edge-sharing octahedra) in the second shell, and a Fe—Fe3 single scattering path (for corner-sharing octahedra) in the third shell. All scattering paths were calculated from the atomic structure of 2-line ferrihydrite (Michel et al., 2007) using the Atoms and FEFF codes, which are incorporated in Artemis. Each scattering path contributed significantly to the final fit. In order to reduce the number of fitting parameters, the following constraints were adopted in the EXAFS model based on the assumed atomic structure and on previous research. The degeneracy of the Fe—O single scattering path was set to 6, and that of the triangular multiple scattering Fe—O—O path to 24. The scattering distance of the Fe—O—O path was constrained to be 1.707 times that of the Fe—O path, and the Debye-Waller factor (or bond-distance distribution parameter, σ^2) of the Fe—O—O path was set equal to that of the Fe—O path, in accordance with Mikutta (2011). The Debye-Waller factors of the Fe—Fe2 and Fe—Fe3 paths were set to 0.0089 and 0.0046 $Å^2$, respectively, which were obtained by fitting the spectrum of 2-line ferrihyrite using the model described here. After the EXAFS experiment, it was noted that self-absorption had occurred due to a high Fe

concentration in the sample (Kelly et al., 2008): if the passive amplitude reduction factor (S_0^2) was fixed at a generally accepted value of 0.72 (Sjöstedt et al., 2013), first-shell fits of our samples yielded very poor fits if the coordination number of Fe-O interactions was fixed to 6, and yielded unrealistically low Fe-O coordination numbers (around 3) if this parameter was not fixed. This adverse phenomenon, which is normally avoided by dilution of the sample in BH_3, was accounted for in the modelling by fitting the amplitude reduction factor. This causes an additional fitting parameter compared to common EXAFS fitting practices. In summary, the EXAFS model had a total of 8 independent fitting parameters: the amplitude reduction factor, the edge energy, the Debye-Waller factor of the Fe—O path, the coordination numbers of the two Fe—Fe paths, and the scattering distances of all three single scattering paths. The number of fitting parameters was, therefore, less than half of the number of independent points in each spectrum.

As an alternative to the shell-by-shell fit of the EXAFS spectra, linear combination fitting (LCF) was performed on k^3-weighted EXAFS spectra in the range k = 2.5—12 $Å^{-1}$. Synthetically produced 2-line ferrihydrite, goethite, lepidocrocite, and Fe(III) complexed by Suwannee River Natural Organic Matter (SRNOM) were selected as standard compounds. The Fe-SRNOM standard was prepared as follows: 50 µg Fe(II) L^{-1} (as $FeSO_4 \cdot 7H_2O$) in aqueous solution was oxidised for 24 hours at pH 7.2 in the presence 10 mg SRNOM L^{-1} and 0.2 mM $NaHCO_3^-$, and the resulting solution was frozen in liquid nitrogen and freeze dried. The iron (hydr)oxides were recorded in transmission mode at MAX-lab (Kleja et al., 2012), whereas the spectrum of the Fe-SRNOM complex was recorded in fluorescence mode. The optimal fits were calculated using a least squares algorithm. The calculated contributions of each standard spectrum were scaled after fitting so that the sum of all contributions equalled 1 in order to account for the self-absorption which occurred in the samples but not in the standards. The self-absorption possibly affected the LCF results to some extent.

3. Results and discussion

The composition and characteristics of water samples are reported in Table 2. The surface waters and groundwaters had a pH between 6.3 and 7.2 and were moderately hard to hard. The surface waters were oxic, whereas the groundwaters were generally anoxic. This is witnessed by the low DO concentration and redox potential as well as by the low NO_3^- and Fe(III) concentrations. Intensive agriculture in the Kleine Nete catchment may promote these reduction processes by inputs of DOM as electron donor. The Fe(II) concentrations in groundwaters varied widely in space and time, which agrees with earlier studies (Van Laer and Smolders, 2013; Vanlierde et al., 2007). In one dataset from earlier studies, the groundwater Fe concentration was negatively correlated with pH, but no such correlation was observed in another dataset. It remains unclear what causes this wide spatiotemporal variation. In selected samples, dissolved Fe(II) concentrations measured by the ferrozine method exceeded the total dissolved Fe concentrations measured by ICP-OES, which was attributed to interferences with the spectrophotometric method, which may be caused by e.g. DOM. The P concentrations in groundwaters were up to 3 mg/L and were more than an order of magnitude larger than those in surface waters (< 0.1 mg/L). This was attributed to coprecipitation with or adsorption on authigenic Fe-rich material. Apart from the concentrations of Fe, NO_3^-, and P, the dissolved composition of groundwater and surface water was quite similar, which reflects that the Kleine Nete catchment is predominantly fed by groundwater. As these groundwaters surface, Fe and P are precipitated, whereas other elements are more conservative. The seasonal variability in groundwater and surface water composition was relatively low, except again for the Fe and P concentrations.

3.1 Oxidation experiments

The oxidation experiments simulated the oxidation of Fe(II) and the formation of authigenic material under conditions representative for those in natural surface waters. The pH was between 6.4 and 7.2 in all treatments. The DO concentrations in all but one of the treatments were between 6 and 10 mg/L, indicating oxic conditions throughout the experiment. In the treatments with only surface water (treatment B), little or no changes in the dissolved concentrations of Fe or other elements were observed during the course of the experiment. In the other treatments, the dissolved Fe(II) concentrations decreased over time. In all but one of the oxidation experiments, the final Fe(II) concentrations were below 10 % of the initial concentrations. The decrease of dissolved Fe(II) was generally accompanied with a decrease in DOC and P, which most likely coprecipitated with Fe. The observed pseudo-first-order oxidation rate of Fe(II) was calculated from the decrease in Fe(II) concentrations over time. The observed rates ranged between 0.01 and 2 h^{-1}. A relatively simple model using the pH, DO concentration, and temperature as inputs (Davison and Seed, 1983) was generally able to predict the Fe(II) oxidation rates within a factor two (see Fig. S6 in the Supplementary Material). More elaborate models for the oxidation rate of Fe(II), which include the effect of various inorganic anions and DOM, have been developed (Craig et al., 2009; e.g. Rose and Waite, 2002), but these complex models have not been widely verified and their application is beyond the scope of this work. The presence of particles and micro-organisms accelerated the oxidation rate of Fe(II) to some extent, but the effect was relatively small (details in section 3 of the Supplementary Material). This suggests that microbial oxidation has only a small effect on the oxidation rate of Fe(II) in the streams. However, in the sediment, the prevailing environmental conditions (DO concentration, microbial diversity, availability of organic matter, water flow rates) are very different from those in the streams, and microbial activity may still play an important role as the groundwater seeps through the sediment into the streams.

Most of the Fe(II) lost from the dissolved phase was recovered as Fe(III) in the particulate (> 0.45 µm) phase. The composition of two authigenic samples are shown in Table 3. The composition of all authigenic samples, mass balances for Fe, the evolution of element concentrations in the dissolved phase, and other details of each oxidation experiment are presented in Tables S4 and S5 in the Supplementary Material. The recovery of Fe was good with losses below 15 %, except in some experiments where adsorption of authigenic material to the recipient walls occurred. The Fe content of the authigenic material produced after oxidation was 44 ± 6 % (average ± standard deviation), which is only slightly lower than the theoretically expected Fe content of a pure HFO phase if a stoichiometry of $Fe(OH)_3$ is assumed (52 %). The difference may be explained by increased hydration and by the presence of other elements which are either adsorbed or incorporated, such as Ca, P, C, and Si. The freshly formed precipitates contained around 1 % of Ca and P. The concentration of P in the freshly formed precipitates decreased as a function of oxidation time. This indicates that P was incorporated in the precipitates that were formed first, an interpretation in line with Voegelin et al. (2010) and with the observed losses of P during storage of groundwater samples (see section 3 of the Supplementary Material). The C concentration was measured in one sample of authigenic material and was 5.4 %. Given the overall decrease in DOC concentrations during the oxidation experiment, it is likely that C was present in all samples of authigenic material. Si may also have been incorporated into authigenic material. Surface waters from the Kleine Nete generally contain around 5 mg Si/L, but Si concentrations have not been measured in the authigenic material. In summary, the oxidation experiments show that, upon oxidation, dissolved Fe(II) in groundwaters causes the production of authigenic material, which contains on average 44 % Fe and smaller amounts of C, Ca, and P, and possibly also Si. In the environment, such authigenic material may be produced in ditches and

small brooks where groundwater surfaces, and it becomes increasingly diluted by allochthonous material as it is transported to streams of increasing order.

3.2 Composition and characteristics of suspended sediment samples

All suspended sediment samples had a reddish brown colour typical for Fe oxides and hydroxides. The composition and particle size of suspended sediment samples (Table 3) was surprisingly constant between samples collected at different times throughout the year. The suspended sediment in the Slootbeek (stream order 2) almost exclusively consisted of Fe (36—40 %), C (9.1—9.7 %), and the associated O and H atoms. Its Fe content was close to the average 44 % Fe that was found in authigenic material, whereas the C content was considerably higher. The mean particle size of the suspended sediment from the Slootbeek was about 3-fold larger than that of authigenic material, which may be a result of ageing: the authigenic material was collected after 48 hours of oxidation, whereas the suspended sediment in the Slootbeek was likely older. The Fe speciation in the Slootbeek and in authigenic material was very similar (EXAFS experiment, see section 3.3). These similarities, together with the fact that the Slootbeek drains an area where groundwater seepage occurs, strongly suggest that the suspended sediment in the Slootbeek almost exclusively consisted of authigenic material.

The suspended sediment samples collected in the Aa (stream order 4) and in the Kleine Nete (stream order 5) had a markedly similar composition. Compared to the suspended sediment in the Slootbeek (stream order 2), these samples contained less Fe (18—26 %) and P (0.8—1.4 %), more other elements such as C (14—17 %) and Si (5—11 %), and their mean particle diameter was about 50 % larger. The molar Fe:P ratios in all suspended sediment samples and in groundwaters were roughly within the same range, which shows that the fate and behaviour of P is linked to that of Fe in the Kleine Nete catchment. The increased concentrations of

elements such as C, Si, Ca, S, and trace metals reflect the increased contribution of additional sources of suspended sediment in the major rivers: a contribution of allochthonous material, and the adsorption of dissolved material (e.g. silicate or organic matter) to the authigenic material.

The average composition of authigenic material was elucidated in the oxidation experiments, but it was difficult to determine the composition of the other end-members based on suspended sediment samples from only 3 locations. Therefore, it was also difficult to estimate the authigenic contribution in the suspended sediment samples. One possibility is to assume that the speciation of allochthonous Fe differs from that of authigenic Fe, e.g. due to glauconite contributions. Since the EXAFS experiment (section 3.3) showed that the Fe speciation in the suspended samples is very well conserved as authigenic material is transported to streams of increasing order, the majority of the Fe in the suspended sediment must then be of authigenic origin. At the upper limit, all Fe in the suspended sediment is authigenic. Using the results from the oxidation experiments, *i.e.* that authigenic material contains on average 44 % Fe, it then follows that the authigenic contribution to the suspended sediment samples from the Aa and Kleine Nete was at most between 41 and 59 %. Another possibility to estimate the authigenic contribution is to use the Fe content of the riverbank material near the sampling locations (6.6 ± 0.8 %; average ± standard error; $n = 4$) as a proxy for the Fe content of allochthonous material. It can then be estimated that the suspended sediment samples from the Aa and Kleine Nete contained between 31 and 52 % authigenic material. These rough estimates (31—59 %) are lower than those of Vanlierde et al. (2007) who estimated the authigenic contribution to the total suspended sediment load between 58 and 96 %. Even though our estimates are somewhat speculative, our study and earlier work show the quantitative importance of authigenic material in the Kleine Nete catchment. An extensive sampling of suspended sediment together with principal component analysis (PCA)

and isotopic fractionation studies might better reveal the composition of the end-members and would allow for a more exact estimate of the authigenic contribution to the total suspended sediment load.

3.3 EXAFS spectroscopy

The measured and fitted k^3-weighted EXAFS spectra (Fig. 1), the magnitude of the Fourier transformed spectra (Fig. 2), and the fitted EXAFS parameters (Table 4) are reported. The analysis of the pre-edge region of the spectra (Prietzel et al., 2007) showed that the Fe is predominantly present as Fe(III) (see Fig. S7 in the Supplementary Material). The EXAFS spectra of suspended sediment and of authigenic material were very similar, and they all resembled that of the ferrihydrite standard. They also resembled the spectrum of a biogenic iron mineral (collected at a hydrothermal vent) very closely (Toner et al., 2009). The spectra clearly differed from that of the goethite and lepidocrocite standards, for example by the features at around 5 and 7.5 $Å^{-1}$. They also differed from that of a Fe-SRNOM complex, although these differences are less clear. The presence of Fe in the form of reduced Fe-S minerals or glauconite must have been limited given the low concentrations of S, Na, K, Mg, and Al (each < 1 %), and therefore these minerals were not included as standards.

All spectra, including that of ferrihydrite, were successfully fitted by the proposed model with two Fe—Fe interactions. The large uncertainties associated with the fit of ferrihydrite are due to the fact that the Debye-Waller factors were fitted, whereas they were fixed while fitting the samples. Various models containing Fe—C interactions were also proposed, but none of them could fit the spectra well. The most notable difference between the samples and ferrihydrite is in the Fourier transformed EXAFS spectra in the region just above 3 Å (Fig. 2). Deconvolution analysis showed that the feature of ferrihydrite in this region, which is less pronounced in the samples, is reflected in the fits by a higher contribution of corner sharing

Fe: the coordination number of Fe—Fe3 was 0.9 for ferrihydrite versus 0.3—0.7 for the samples (Table 4). The great overall similarity between all spectra shows that the Fe speciation in the authigenic material was very similar to that in the suspended sediment samples. This suggests that the Fe in suspended sediment indeed predominantly originated from oxidising groundwaters. However, subtle differences exist between the samples: the suspended sediment samples isolated in the field had higher Fe—Fe2 and Fe—Fe3 coordination numbers than the authigenic material, *i.e.* the authigenic material is less hydrolysed compared to downstream samples. This different degree of hydrolysis may reflect ageing effects: the authigenic material was very fresh (48 hours old), whereas the suspended sediment samples likely were somewhat older. The results of the LCF analysis are generally in line with these findings. The LCF analysis predicts that ferrihydrite (67—82 %) is the dominant species, with smaller contributions of Fe-SRNOM complexes (8—26 %) and of lepidocrocite (4—15 %) (see Table S6 in the Supplementary Material). Our findings are in line with earlier work which showed that the oxidation of Fe(II) predominantly yields ferrihydrite in the presence of around 5 mg Si/L, a concentration typical of waters from the Kleine Nete catchment (Tipping et al., 1989; Voegelin et al., 2010). To conclude, the EXAFS experiment shows that the Fe in authigenic material is predominantly present as poorly crystalline oxyhydroxides such as ferrihydrite, and that the Fe speciation is well conserved as the material is transported downstream to rivers of increasing order.

One objective of this EXAFS experiment was to elucidate subtle differences in Fe coordination numbers between our samples. The same relatively simple atomic structure and EXAFS model was therefore applied to all samples. We admit that our model ignored some interatomic interactions that were present in the EXAFS signal. However, the selection of more elaborate models would likely lead to different models for each sample, which reduces the comparability of the results: detected differences in Fe—Fe coordination numbers may

then be due to model differences rather than true differences in Fe speciation. This justifies the selection of a simple EXAFS model within the context of this study.

A general problem in EXAFS analysis is that coordination numbers and Debye-Waller factors are correlated. In recent studies on Fe-EXAFS spectra of environmental samples with a structure similar to that of ferrihydrite, different approaches have been adopted in order to derive Fe—Fe coordination numbers. Some authors have fitted the Debye-Waller factors together with coordination numbers (Gustafsson et al., 2007; Toner et al., 2009; and this study), others have fixed the Debye-Waller factors at literature values of ferrihydrite or goethite (Karlsson and Persson, 2010; Karlsson et al., 2008), in some cases averaged over different studies (Mikutta et al., 2010), and still others have fitted the Debye-Waller factors for ferrihydrite and used these as fixed parameters for their samples (Karlsson and Persson, 2012; Kleja et al., 2012; Mikutta, 2011; Sjöstedt et al., 2013). Whichever approach is used, the derivation or choice of Debye-Waller factors remains inherently uncertain. The reported Debye-Waller factors and coordination numbers for Fe—Fe interactions in ferrihydrite vary widely (Table 5). Kleja et al. (2012) interpreted this as variability of ferrihydrite at the nanoscale, but another explanation may be the inherent uncertainty in modelling the ferrihydrite EXAFS signal and the correlation between Debye-Waller factors and coordination numbers. Among the 10 ferrihydrite samples in Table 5 that have been fitted with two Fe—Fe distances, there is a correlation ($R^2 = 0.61$; $P = 0.008$) between the Debye-Waller factors and the coordination numbers of the Fe—Fe distance at around 3.03 Å. This correlation is even stronger if the fit by Sjöstedt et al. (2013), who fixed the coordination numbers contrary to the other studies, is excluded ($R^2 = 0.79$; $P = 0.001$). For the Fe—Fe distance at around 3.43 Å, there is no such correlation. In this work, relatively low Debye-Waller factors are obtained for ferrihydrite, but if for example the values obtained by Mikutta (2011) are used, the fitted Fe—Fe coordination numbers in the samples increase by factors

between 1.4 and 2, but the observed trends and differences between the samples remain largely unaffected. It is concluded that the choice of the Debye-Waller factors for ferrihydrite-like samples is somewhat arbitrary. The reported coordination numbers may be compared between different samples to yield valuable information, but they have little significance in absolute terms.

4. Conclusions

Taken together, we showed that the surfacing of Fe-rich groundwaters from the Kleine Nete catchment removed Fe(II) together with DOC and P from the dissolved phase. The Fe(III) precipitated and formed authigenic material, which contained 44 ± 6 % Fe (average ± standard deviation) and smaller quantities of adsorbed or incorporated elements such as C, P, Ca, and possibly also Si. The Fe was in the form of poorly crystalline hydrous ferric oxides with a structure similar to ferrihydrite. The mean particle size of 48-hour old authigenic material was between 3 and 4 µm. Phosphorus was very efficiently bound by authigenic material, as evidenced by the strong decrease in dissolved P concentrations in oxidising groundwaters.

The authigenic material becomes part of the suspended sediment and is transported to streams of increasing order. The suspended sediment in a small brook draining a groundwater seepage area (Slootbeek, stream order 2) almost exclusively consisted of authigenic material. Its composition (36—40 % Fe) and Fe speciation were very similar to those of authigenic material. Further downstream, in streams of order 4 (Aa) and 5 (Kleine Nete), the authigenic material becomes increasingly diluted by allochthonous material, and possibly also by increased adsorption of dissolved constituents onto authigenic material. This results in decreasing Fe (18—26 %) and P concentrations, and increasing concentrations of other elements such as C, Si, Ca, Al, and trace metals. Apart from the changing composition, the downstream transport was also accompanied by an increase in mean particle size and in hydrolysis of Fe. These effects may be the result of ageing of authigenic material. The contribution of authigenic material to the suspended sediment samples from the streams of order 4 and 5 was estimated at between 31 and 59 %. However, a more extensive sampling of suspended sediment together with principal component analysis is needed to refine these estimates.

Acknowledgements

S.B. thanks the Research Foundation Flanders (FWO) for a PhD fellowship, and the FWO and the FIMIN research networking programme of the European Science Foundation (ESF) for travel grants. The EXAFS experiments were carried out at beamline I811, MAX-lab synchrotron radiation source, Lund University, Sweden – thanks to Ingmar Persson and the beamline I811 staff. Funding for the beamline I811 project was kindly provided by The Swedish Research Council and The Knut and Alice Wallenberg Foundation. Ed Tipping, Tim Mansfeldt, Peter Salaets and Danny Wilczek are acknowledged for their help. Financial support was provided by Flanders Hydraulics Research (Waterbouwkundig Laboratorium; project number 613_10aMARS), a division of the Department of Mobility and Public Works of the Flemish Government - thanks to Elin Vanlierde, Frank Mostaert, and others who have contributed to this project.

Appendix A. Supplementary Material

Supplementary Material associated with this article can be found, in the online version, at <insert URL here>.

References

Boyle, E.A., Edmond, J.M., Sholkovitz, E.R., 1977. The mechanism of iron removal in estuaries. Geochim. Cosmochim. Acta 41, 1313–1324.

Carlson, S., Clausén, M., Gridneva, L., Sommarin, B., Svensson, C., 2006. XAFS experiments at beamline I811, MAX-lab synchrotron source, Sweden. J. Synchrotron Radiat. 13, 359–364.

Châtellier, X., West, M.M., Rose, J., Fortin, D., Leppard, G.G., Ferris, F.G., 2004. Characterization of iron oxides formed by oxidation of ferrous ions in the presence of various bacterial species and inorganic ligands. Geomicrobiol. J. 21, 99–112.

Combes, J.M., Manceau, A., Calas, G., 1990. Formation of ferric oxides from aqueous solutions: A polyhedral approach by X-ray Absorption Spectroscopy: II. Hematite formation from ferric gels. Geochim. Cosmochim. Acta 54, 1083–1091.

Courbe, C., Velde, B., Meunier, A., 1981. Weathering of glauconites: Reversal of the glauconitization process in a soil profile in Western France. Clay Miner. 16, 231–243.

Craig, P.S., Shaw, T.J., Miller, P.L., Pellechia, P.J., Ferry, J.L., 2009. Use of multiparametric techniques to quantify the effects of naturally occurring ligands on the kinetics of Fe(II) oxidation. Environ. Sci. Technol. 43, 337–42.

Davison, W., Seed, G., 1983. The kinetics of the oxidation of ferrous iron in synthetic and natural waters. Geochim. Cosmochim. Acta 47, 67–79.

De Geyter, G., Vandenberghe, R.E., Verdonck, L., Stoops, G., 1985. Mineralogy of holocene bog-iron ore in northern Belgium. Neues Jahrbuch für Mineralogie - Abhandlungen 153, 1–17.

De Vet, W.W.J.M., Dinkla, I.J.T., Rietveld, L.C., van Loosdrecht, M.C.M., 2011. Biological iron oxidation by Gallionella spp. in drinking water production under fully aerated conditions. Water Res. 45, 5389–98.

Dzombak, D.A., Morel, F.M.M., 1990. Surface complexation modeling: Hydrous ferric oxide. Wiley-Interscience, New York.

Gunnars, A., Blomqvist, S., Johansson, P., Andersson, C., 2002. Formation of Fe(III) oxyhydroxide colloids in freshwater and brackish seawater, with incorporation of phosphate and calcium. Geochim. Cosmochim. Acta 66, 745–758.

Gustafsson, J.P., Persson, I., Kleja, D.B., Van Schaik, J.W.J., 2007. Binding of iron(III) to organic soils: EXAFS spectroscopy and chemical equilibrium modeling. Environ. Sci. Technol. 41, 1232–7.

Hansel, C.M., Wielinga, B.W., Fendorf, S., 2003. Structural and compositional evolution of Cr/Fe solids after indirect chromate reduction by dissimilatory iron-reducing bacteria. Geochim. Cosmochim. Acta 67, 401–412.

Huser, B.J., Köhler, S.J., Wilander, A., Johansson, K., Fölster, J., 2011. Temporal and spatial trends for trace metals in streams and rivers across Sweden (1996–2009). Biogeosciences 8, 1813–1823.

Hyacinthe, C., Van Cappellen, P., 2004. An authigenic iron phosphate phase in estuarine sediments: composition, formation and chemical reactivity. Mar. Chem. 91, 227–251.

Karlsson, T., Persson, P., 2010. Coordination chemistry and hydrolysis of Fe(III) in a peat humic acid studied by X-ray absorption spectroscopy. Geochim. Cosmochim. Acta 74, 30–40.

Karlsson, T., Persson, P., 2012. Complexes with aquatic organic matter suppress hydrolysis and precipitation of Fe(III). Chem. Geol. 322-323, 19–27.

Karlsson, T., Persson, P., Skyllberg, U., Mörth, C.-M., Giesler, R., 2008. Characterization of iron(III) in organic soils using extended X-ray absorption fine structure spectroscopy. Environ. Sci. Technol. 42, 5449–54.

Kelly, S., Hesterberg, D., Ravel, B., 2008. Analysis of soils and minerals using X-ray absorption spectroscopy, in: Methods of Soil Analysis. pp. 387–464.

Kleja, D.B., van Schaik, J.W.J., Persson, I., Gustafsson, J.P., 2012. Characterization of iron in floating surface films of some natural waters using EXAFS. Chem. Geol. 326-327, 19–26.

Lienemann, C.-P., Monnerat, M., Dominik, J., Perret, D., 1999. Identification of stoichiometric iron-phosphorus colloids produced in a eutrophic lake. Aquat. Sci. 61, 133.

Lofts, S., Tipping, E., Hamilton-Taylor, J., 2008. The chemical speciation of Fe(III) in freshwaters. Aquat. Geochem. 14, 337–358.

Maillot, F., Morin, G., Wang, Y., Bonnin, D., Ildefonse, P., Chaneac, C., Calas, G., 2011. New insight into the structure of nanocrystalline ferrihydrite: EXAFS evidence for tetrahedrally coordinated iron(III). Geochim. Cosmochim. Acta 75, 2708–2720.

Michel, F.M., Ehm, L., Antao, S.M., Lee, P.L., Chupas, P.J., Liu, G., Strongin, D.R., Schoonen, M.A.A., Phillips, B.L., Parise, J.B., 2007. The structure of ferrihydrite, a nanocrystalline material. Science 316, 1726–1729.

Mikutta, C., 2011. X-ray absorption spectroscopy study on the effect of hydroxybenzoic acids on the formation and structure of ferrihydrite. Geochim. Cosmochim. Acta 75, 5122–5139.

Mikutta, C., Frommer, J., Voegelin, A., Kaegi, R., Kretzschmar, R., 2010. Effect of citrate on the local Fe coordination in ferrihydrite, arsenate binding, and ternary arsenate complex formation. Geochim. Cosmochim. Acta 74, 5574–5592.

O'Day, P.A., Rivera, N., Root, R., Carroll, S.A., 2004. X-ray absorption spectroscopic study of Fe reference compounds for the analysis of natural sediments. Am. Mineral. 89, 572–585.

Perret, D., Gaillard, J.-F., Dominik, J., Atteia, O., 2000. The diversity of natural hydrous iron oxides. Environ. Sci. Technol. 34, 3540–3546.

Prietzel, J., Thieme, J., Eusterhues, K., Eichert, D., 2007. Iron speciation in soils and soil aggregates by synchrotron-based X-ray microspectroscopy (XANES, μ-XANES). Eur. J. Soil Sci. 58, 1027–1041.

Ravel, B., Newville, M., 2005. ATHENA, ARTEMIS, HEPHAESTUS: data analysis for X-ray absorption spectroscopy using IFEFFIT. J. Synchrotron Radiat. 12, 537–41.

Rhoton, F.E., Bigham, J.M., Lindbo, D.L., 2002. Properties of iron oxides in streams draining the Loess Uplands of Mississippi. Appl. Geochem. 17, 409–419.

Rose, A.L., Waite, T.D., 2002. Kinetic model for Fe(II) oxidation in seawater in the absence and presence of natural organic matter. Environ. Sci. Technol. 36, 433–44.

Salminen, R. (Ed.), 2005. Geochemical Atlas of Europe. Part 1: Background Information, Methodology and Maps. Geological Survey of Finland, Espoo, Finland.

Schindler, D.W., 2012. The dilemma of controlling cultural eutrophication of lakes. Proc. Biol. Sci. 279, 4322–33.

Sjöstedt, C., Persson, I., Hesterberg, D., Kleja, D.B., Borg, H., Gustafsson, J.P., 2013. Iron speciation in soft-water lakes and soils as determined by EXAFS spectroscopy and geochemical modelling. Geochim. Cosmochim. Acta 105, 172–186.

Tipping, E., Thompson, D.W., Woof, C., 1989. Iron oxide particulates formed by the oxygenation of natural and model lakewaters containing Fe(II). Archiv für Hydrobiologie 115, 59–70.

Toner, B.M., Santelli, C.M., Marcus, M.A., Wirth, R., Chan, C.S., McCollom, T., Bach, W., Edwards, K.J., 2009. Biogenic iron oxyhydroxide formation at mid-ocean ridge hydrothermal vents: Juan de Fuca Ridge. Geochim. Cosmochim. Acta 73, 388–403.

Van Laer, L., Smolders, E., 2013. Does soil water saturation mobilize metals from riparian soils to adjacent surface water? A field monitoring study in a metal contaminated region. Environ. Sci. Process. Impacts 15, 1181–1190.

Vanlierde, E., De Schutter, J., Jacobs, P., Mostaert, F., 2007. Estimating and modeling the annual contribution of authigenic sediment to the total suspended sediment load in the Kleine Nete Basin, Belgium. Sediment. Geol. 202, 317–332.

Viollier, E., Inglett, P.W., Hunter, K., Roychoudhury, A.N., Van Cappellen, P., 2000. The ferrozine method revisited: Fe(II)/Fe(III) determination in natural waters. Appl. Geochem. 15, 785–790.

Vlaamse Milieumaatschappij VMM, 2013. Geoloket Waterkwaliteit (http://www.vmm.be/geoview). Accessed on 05/03/2013 [WWW Document].

Voegelin, A., Kaegi, R., Frommer, J., Vantelon, D., Hug, S.J., 2010. Effect of phosphate, silicate, and Ca on Fe(III)-precipitates formed in aerated Fe(II)- and As(III)-containing water studied by X-ray absorption spectroscopy. Geochim. Cosmochim. Acta 74, 164–186.

Wällstedt, T., Björkvald, L., Gustafsson, J.P., 2010. Increasing concentrations of arsenic and vanadium in (southern) Swedish streams. Appl. Geochem. 25, 1162–1175.

Waychunas, G.A., Rea, B.A., Fuller, C.C., Davis, J.A., 1993. Surface chemistry of ferrihydrite: Part 1. EXAFS studies of the geometry of coprecipitated and adsorbed arsenate. Geochim. Cosmochim. Acta 57, 2251–2269.

Table 1: Treatments included in the oxidation experiments.

Code	Prefiltration	Treatment
A	yes	Only groundwater
B	yes	Only surface water
C	yes	1:1 mix of groundwater + surface water
D	yes	Surface water spiked with Fe(II)
E	no	1:1 mix of groundwater + surface water
F	no	Surface water spiked with Fe(II)
G	no	Surface water spiked with Fe(II) and formalin

Table 2: Characteristics and composition of surface water and groundwater samples. The concentrations of elements and anions were measured after membrane filtration (0.45 µm).

	Sampling event	pH	EC *µS/cm*	DO *mg/L*	ORP *mV*	Fe(II) *mg/L*	total Fe *mg/L*	Na *mg/L*	Mg *mg/L*	K *mg/L*	Ca *mg/L*	P *mg/L*	DOC *mg/L*	DIC *mg/L*	Cl^- *mg/L*	SO_4^{2-} *mg/L*	NO_3^- *mg/L*	SS *mg/L*	Q m^3/s
Slootbeek	S1	6.7	314	5.7	282	nm	0.04	8.1	4.7	7.9	26.3	nm	3.3	13.4	nm	nm	nm	5.7	nm
surface water	S2	6.4	369	5.5	179	9.56	9.82	12.0	5.8	7.7	38.3	0.07	7.2	16.3	30	54	2.6	20.2	nm
(stream order 2)	S4	6.7	300	5.8	278	0.55	0.72	11.2	5.7	7.9	41.8	0.02	13.4	19.0	33	51	2.0	41.8	nm
Aa	S1	7.2	546	8.1	321	nm	0.12	41.8	5.4	12.9	42.0	nm	8.2	26.7	70	46	13.6	6.3	3.6
surface water	S2	6.8	400	7.4	184	0.52	1.21	20.9	5.6	10.3	40.4	0.08	14.3	20.3	35	48	9.7	21.1	4.5
(stream order 4)	S3	7.2	nm	6.8	309	0.35	0.41	27.1	5.6	10.1	47.9	0.02	10.3	25.8	51	56	8.6	nm	2.1
	S4	7.1	391	6.7	257	0.07	1.06	22.7	5.5	11.3	47.8	0.09	12.8	24.0	46	57	8.2	9.5	nm
Aa	S1	6.8	692	0.3	103	nm	nm	46.4	4.7	7.2	49.3	nm	7.1	35.8	78	26	<0.1		
groundwater	S2	6.3	751	0.4	124	58.0	53.8	25.1	4.5	5.6	78.7	2.18	16.8	26.5	92	51	0.6		
	S3	6.5	nm	0.5	129	28.1	28.0	42.9	2.8	5.4	42.2	3.00	11.8	23.5	73	36	<0.1		
	S4	6.4	593	0.3	112	36.7	33.2	35.6	3.8	7.5	61.4	3.07	16.1	21.8	93	83	0.4		
Kleine Nete	S1	7.0	531	9.2	385	nm	0.17	50.2	6.2	8.5	35.7	nm	7.4	16.5	57	95	5.9	9.5	4.4
surface water	S2	7.0	487	11.1	334	0.09	0.96	57.8	6.7	9.4	35.1	0.09	9.7	14.1	62	118	7.9	29.6	0.7
(stream order 5)	S3	7.1	376	11.8	408	0.17	0.25	24.5	5.6	8.2	35.1	0.03	7.3	14.6	45	55	6.8	8.1	3.4
	S4	7.0	595	7.2	440	0.09	0.80	54.0	6.7	10.1	34.2	0.07	10.6	15.1	93	129	8.2	4.2	1.1
Kleine Nete	S1	6.8	649	0.3	101	nm	nm	72.9	4.3	8.7	29.7	nm	6.1	17.2	80	100	0.3		
groundwater	S2	6.8	581	0.5	115	14.9	15.2	66.7	5.5	6.8	34.9	0.61	14.5	23.9	68	86	0.2		
	S3	6.7	569	2.4	200	3.81	3.47	52.4	5.3	8.9	34.5	0.12	8.0	15.5	75	106	<0.1		
	S4	6.9	655	0.4	191	9.24	8.86	74.5	4.9	8.2	33.8	0.64	10.6	24.6	97	124	0.4		

nm: not measured; EC: electric conductivity; DO: disolved oxygen; ORP: oxido-reduction potential; DOC: dissolved organic carbon; DIC: dissolved inorganic carbon; SS: suspended sediment; Q: discharge

Table 3: Composition and particle size distribution of authigenic material and of suspended sediment from streams of increasing order. The authigenic samples presented are those used in EXAFS analysis; the composition of other authigenic samples is presented in Tables S4 and S5 in the Supplementary Material. The suspended sediment data are the average ± standard deviation of samples isolated at four moments throughout the year.

	sample[$]	C	Fe	Si	P	Al	Ca	S	Fe:P	P_{10}	P_{50}	P_{90}
		%	*%*	*%*	*%*	*%*	*%*	*g/kg*	*mol/mol*	*µm*	*µm*	*µm*
AUTHIGENIC MATERIAL	oxidised groundwater (A)	5.4	37.3	nm	1.4	< 0.5	1.08	nm	15	1.0	4.1	18.2
	oxidised groundwater + surface water (C)	nm	36.9	nm	1.1	< 0.5	0.99	nm	19	0.3	2.9	21.3
SUSPENDED SEDIMENT	Slootbeek (stream order 2)	9.4±0.3	37.1±2.6	2.9±0.2	2.0±0.4	0.3±0.1	0.9±0.02	2.6±0.5	11±3	2.7±0.6	10.9±0.4	43.4±3.1
	Aa (stream order 4)	16.4±1.4	20.0±2.4	7.4±3.4	1.2±0.2	1.3±0.5	1.8±0.1	5.8±0.2	10±2	4.4±0.5	18.8±1.6	85.7±13.5
	Kleine Nete (stream order 5)	15.1±1.0	24.1±1.3	5.6±0.4	1.1±0.2	1.2±0.3	1.5±0.2	6.7±1.7	13±2	4.2±0.3	16.4±1.5	72.4±13.6

nm: not measured

[$] Characters between brackets refer to treatments in the oxidation experiments

P_x: x^{th} percentile of the volume-weighted particle size distribution expressed as the particle diameter

Table 4: Fitted parameters and uncertainties for the EXAFS spectra of 48-hour old authigenic material, suspended sediment samples, and ferrihydrite.

sample[$]	Red χ^2	E_0 (eV)	S_0^2	Fe—O			Fe—Fe2			Fe—Fe3			Fe—O—O^		
				N	R (Å)	σ^2 (Å^2)	N	R (Å)	σ^2 (Å^2)	N	R (Å)	σ^2 (Å^2)	N	R (Å)	σ^2 (Å^2)
Oxidised groundwater (A)	1196	-0.32	0.45	6*	1.97	0.0077	1.6	3.04	0.0089*	0.3	3.44	0.0046*	24*	3.37	0.0077
					±0.01	±0.0011	±0.4	±0.02		±0.3	±0.07				
Oxidised groundwater + surface water (C)	1343	0.01	0.29	6*	1.98	0.0079	1.8	3.04	0.0089*	0.4	3.45	0.0046*	24*	3.37	0.0079
					±0.01	±0.0013	±0.5	±0.02		±0.4	±0.06				
Slootbeek (stream order 2)	963	0.72	0.29	6*	1.98	0.0077	2.5	3.04	0.0089*	0.7	3.44	0.0046*	24*	3.38	0.0077
					±0.01	±0.0015	±0.6	±0.02		±0.5	±0.05				
Aa (stream order 4)	866	0.67	0.39	6*	1.98	0.0071	2.2	3.05	0.0089*	0.6	3.43	0.0046*	24*	3.38	0.0071
					±0.01	±0.0014	±0.6	±0.02		±0.5	±0.05				
Kleine Nete (stream order 5)	808	0.80	0.36	6*	1.99	0.0078	2.8	3.05	0.0089*	0.7	3.43	0.0046*	24*	3.39	0.0078
					±0.01	±0.0012	±0.5	±0.01		±0.4	±0.04				
Ferrihydrite	1043	-0.20	0.72	6*	1.97	0.0099	1.6	3.02	0.0089	0.9	3.45	0.0046	24*	3.37	0.0099
					±0.01	±0.0015	±1.2	±0.03		±0.9	±0.03				

$ Characters between brackets refer to treatments in the oxidation experiments
Red χ^2: reduced chi-square statistic
E_0: edge energy
S_0^2: passive amplitude reduction factor
N: coordination number
R: interatomic distance
σ^2: Debye-Waller factor or bond distance distribution
* parameter fixed during fitting
^ For the triangular Fe—O—O multiple scattering path, R was constrained to be 1.707 times that of the Fe—O path, and σ^2 was constrained to equal that of the Fe—O path.

Table 5: Literature overview of fitted Debye-Waller factors (σ^2) for Fe—Fe interactions in ferrihydrite. Interactions around 3.03 Å refer to edge sharing Fe—Fe linkages; interactions around 3.43 Å refer to corner sharing Fe—Fe linkages.

Sample	Reference	R (Å)	N	σ^2 (Å^2)	R (Å)	N	σ^2 (Å^2)	R (Å)	N	σ^2 (Å^2)	notes
Ferrihydrite	(Mikutta, 2011)	3.06	3.4	0.013				3.47	1.7	0.007	
2-line ferrihydrite	(Kleja et al., 2012)	3.03	2.2	0.0092				3.49	4.3	0.0112	
Ferrihydrite	(Mikutta et al., 2010)	3.03	1.4	0.009*				3.45	1.3	0.009*	σ^2 is a literature average
Ferrihydrite	(Hansel et al., 2003)	3.02	2.0	0.008				3.43	3.5	0.009	
HFO gel	(Combes et al., 1990)	3.06	3.5	0.0144				3.43	1.5	0.0121	
Ferrihydrite	(Waychunas et al., 1993)	3.00—3.05	1.3—1.9	0.0049				3.41—3.45	1.4—2.6	0.0049	
Ferrihydrite	(Karlsson and Persson, 2012)	2.98	2.8	0.0109				3.41	1.1	0.0046	
2-line ferrihydrite	(Toner et al., 2009)	3.05	3.5	0.013				3.45	1.4	0.006	
2-line ferrihydrite	(Sjöstedt et al., 2013)	3.04	2*	0.013				3.44	4*	0.0065	
2-line ferrihydrite	(Maillot et al., 2011)	3.00	1.3	0.01	3.12	1.1	0.01	3.45	2.2	0.01	σ^2 set identical for all three shells
2-line ferrihydrite	(O'Day et al., 2004)	3.02—3.03	2*	0.0030—0.0040	3.24	2*	0.0151—0.0179	3.41—3.42	4*	0.0088—0.0092	
2-line ferrihydrite	this study	3.02	1.6	0.0089				3.45	0.9	0.0046	

HFO Hydrous Ferric Oxide

N: coordination number

R: interatomic distance

σ^2: Debye-Waller factor or bond distance distribution

* parameter fixed during fitting

Figures

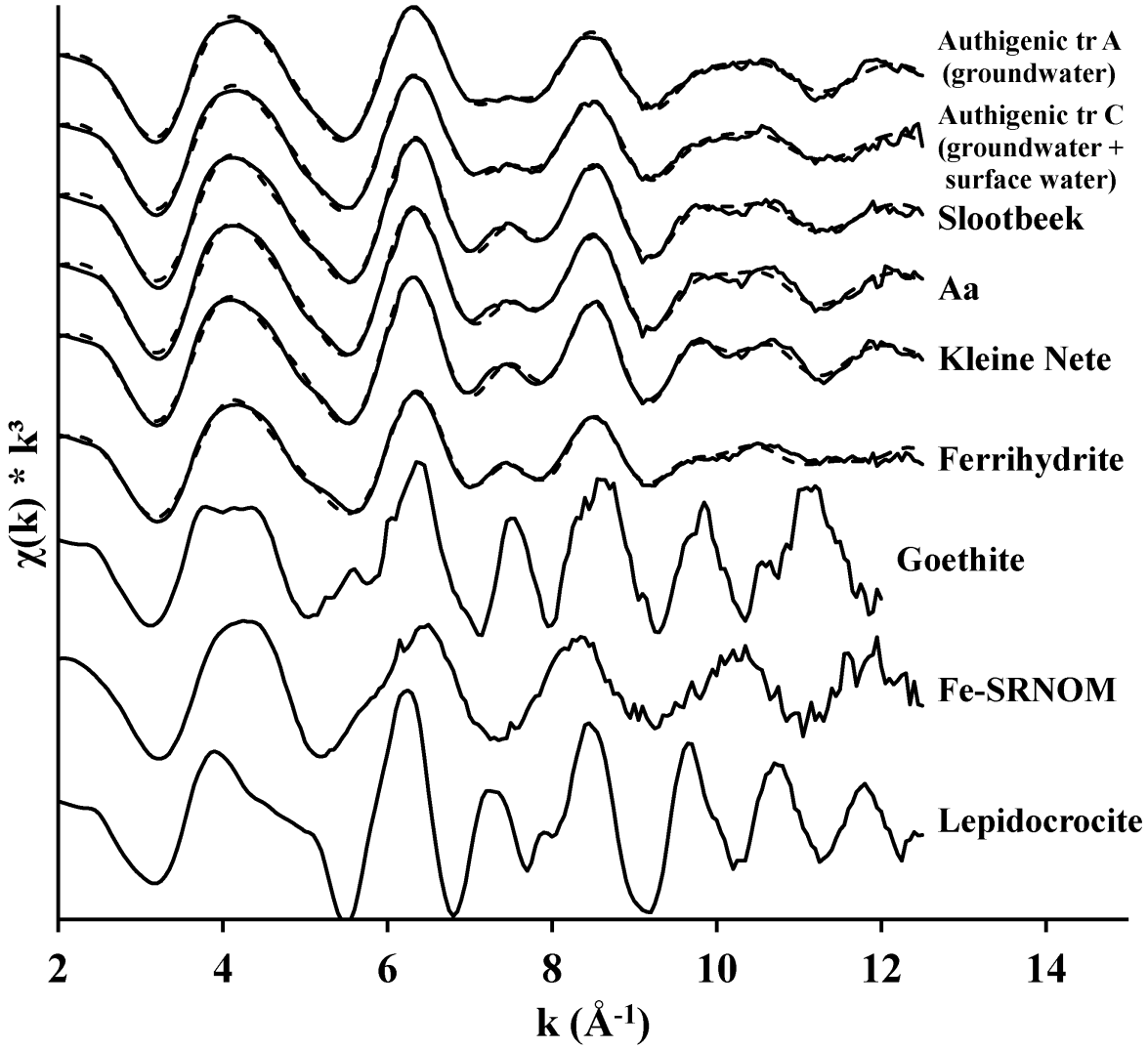

Figure 1: Measured (full lines) and fitted (dashed lines) k^3-weighted Fe EXAFS spectra of authigenic material and of suspended sediment from rivers of increasing order. All spectra were divided by their fitted amplitude reduction factors for easier visual comparison.

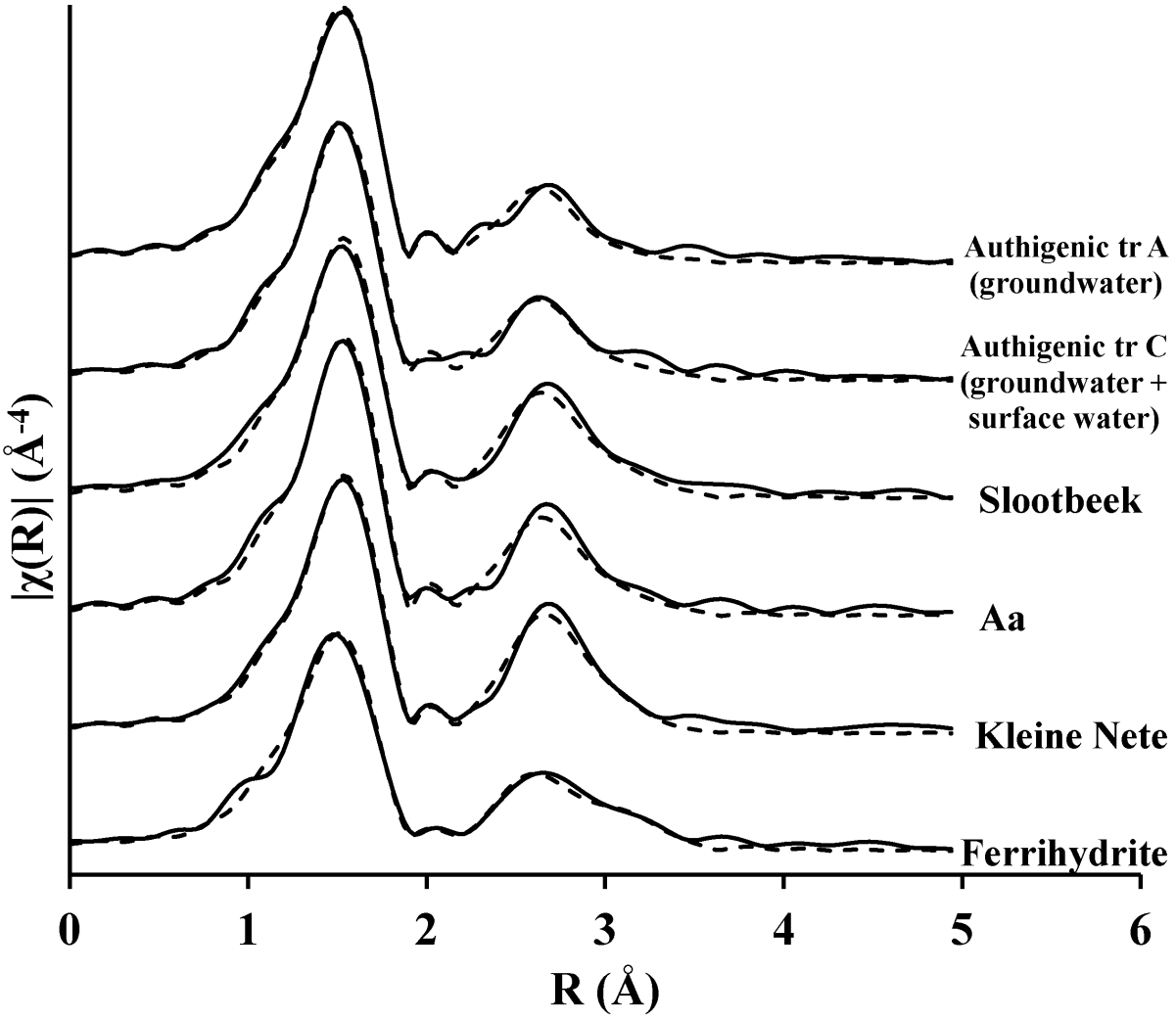

Figure 2: Magnitude of measured (full lines) and fitted (dashed lines) Fourier transformed k^3-weighted Fe EXAFS spectra of authigenic material and of suspended sediment from rivers of increasing order. All spectra were divided by their fitted amplitude reduction factors for easier visual comparison.